CHEMISTRY
A EUROPEAN JOURNAL

Supporting Information

Organolanthanide-Mediated Intermolecular Hydroamination of 1,3-Dienes: Mechanistic Insights from a Computational Exploration of Diverse Mechanistic Pathways for the Stereoselective Hydroamination of 1,3-Butadiene with a Primary Amine Supported by an *Ansa*-Neodymocene-Based Catalyst

Sven Tobisch,*[a]

[a] Institut für Anorganische Chemie der Martin-Luther-Universität Halle-Wittenberg, Fachbereich Chemie, Kurt-Mothes-Straße 2, D-06120 Halle, Germany
E-mail: tobisch@chemie.uni-halle.de

Computational Details

Method. All calculations have been performed with the program package TURBOMOLE[1] using density functional theory (DFT). The local exchange-correlation potential by Slater[2a,b] and Vosko et al.[2c] was augmented with gradient-corrected functionals for electron exchange according to Becke[2d] and correlation according to Perdew[2e] in a self-consistent fashion. This gradient-corrected density functional is usually termed BP86 in the literature and was shown to be able to describe both energetic and structural aspects of organolanthanide compounds reliably.[3] The suitability of the BP86 functional for the reliable determination of the energy profile for organolanthanide-supported catalytic transformations has been demonstrated in previous studies,[4] and this allows mechanistic conclusions having substantial predictive value to be drawn. In view of the fact that all species investigated in this study show a large HOMO–LUMO gap, a spin-restricted formalism was used for all the calculations.

Two different basis set levels (basis set A, B) were adopted throughout the present investigation, employing the same description of the lanthanide atom. For Nd we used the Stuttgart–Dresden quasirelativistic effective core potential (SDD) with the associate (7s6p5d)/[5s4p3d] valence basis set contracted according to a (31111/3111/311) scheme.[5] This ECP treats [Kr]$4d^{10}4f^{3}$ as a fixed core, whereas $5s^{2}5p^{6}6s^{2}5d^{1}6p^{0}$ shells are taken into account explicitly. First, as far as basis set A is regarded, all other elements were represented by Ahlrichs' split-valence SV(P) basis set[6a] with polarization functions on heavy main group atoms, but not on hydrogen; namely, for carbon and nitrogen a 7s/4p/1d set contracted to (511/31/1) and for hydrogen a 4s set contracted to (31). The second more accurate basis set B, consists of Ahlrichs' valence triple-ζ TZVP basis set[6b] with polarization functions on all main group atoms; namely, for carbon and nitrogen a 11s/6p/1d set contracted to (62111/411/1) and for hydrogen a 5s/1p set contracted to (311/1).

Stationary Points. The geometry optimization and the saddle-point search were carried out by utilizing analytical/numerical gradients/Hessians according to standard algorithms. No symmetry constraints were imposed in any case. The stationary points located by using basis set A were identified exactly by the curvature of the potential-energy surface at these points corresponding to the eigenvalues of the Hessian. This level of basis-set quality has been identified as a reliable tool for the assessment of structural parameters and vibrational frequencies.[7] All reported transition states possess exactly one negative Hessian eigenvalue,

while all other stationary points exhibit exclusively positive eigenvalues. Each transition state was further confirmed by following its imaginary vibrational mode downhill on both sides from slightly distorted TS structures, yielding to the reactant and product minima presented on the reaction profile for the individual steps. Visual inspection of imaginary vibrational modes was performed with the STRUKED program.[8] The many isomers that are possible for each of the investigated species were carefully explored. The reaction and activation enthalpies and free energies (ΔH, $\Delta H^{\ddagger}$ and ΔG, $\Delta G^{\ddagger}$ at 298 K and 1 atm) were evaluated according to standard textbook procedures[9] using harmonic frequencies that were computed at basis set A level. To obtain more accurate energy profiles, all key species were fully located by employing basis set B.

It has been explicitly scrutinized for each of the individual steps in Scheme 2 whether a specific reactant species, which are always available in excess,[10] is likely to facilitate the elementary process. Furthermore, the influence of nonspecific solute–solvent interactions[11] on the energy profile of individual steps has been estimated for benzene[10] (dielectric constant ε = 2.247 at 298 K)[12] by employing the conductor-like screening model (COSMO) due to Klamt and Schüürmann[13] as implemented in TURBOMOLE.[14] Nonelectrostatic contributions to solvation were not considered. The solvation effects were included selfconsistently in the calculations, and all key species were fully optimized including solvation at the BP86 basis set B level. The optimized atomic COSMO radii (r_H = 1.3 Å, r_C = 2.0 Å, r_N = 1.83 Å, r_{Si} = 2.46 Å)[15] have been used, in combination with the non-optimized radius of 2.22 Å for Nd.

Energetics (BP86(COSMO)/basis set B) on the ΔH(298 K) surface were reported as ΔE plus zero point energy correction at 0 K plus thermal motion corrections at 298 K plus solvation correction. The Gibbs free-energies were obtained as $\Delta G_{298} = \Delta H_{298} - T\Delta S$ at 298 K and 1 atm. The $T\Delta S$ contribution of about 11–13 kcal mol^{-1} (under standard conditions) calculated for butadiene and amine substrate coordination in gas phase certainly does not reflect the real entropic cost for substrate association/dissociation processes under actual catalytic conditions.[10] The difference in the reaction entropy for the $Me_2SiCp'_2LnR$ + **1** → $Me_2SiCp'_2LnR$–**1** substrate uptake process taking place in the gas and condensed phases is mainly due to the substrate solvation, since the solvation entropies of the $Me_2SiCp'_2LnR$ species and the $Me_2SiCp'_2LnR$–**1** adduct can be regarded as being similar. The solvation entropy of ethylene is about 16 cal mol^{-1} K^{-1} in typical aromatic hydrocarbon solvents,[16] which can reasonably be adopted as a rough estimate for butadiene and amines as well. This reduces the entropic costs for substrate complexation by about 4.8 kcal

mol^{-1} (298.15 K); thus to about two-thirds of the gas-phase value. This estimation agrees reasonably well with the findings of a recent theoretical study, where it was shown that for polar solvents the entropies in solution decrease to nearly half of the gas-phase value.[17] Therefore, the solvation entropy for substrate association and dissociation was approximated as being two-thirds of its gas-phase value, which the author considers as a reliable estimate of the entropy contribution in the condensed phase.

Labeling of the Molecules. Important species of the catalytic cycle were labeled with the Arabic numbers given in Scheme 2. Please note that the diene-amido–Ln active catalyst complex **4** is omitted in Scheme 2. In addition to the various regio- and stereoisomeric pathways for each of the individual steps shown in Scheme 2, it was explicitly scrutinized, which of the two enantiofaces (*re*/*si*)[18] of the prochiral 1,3-butadiene is involved along the minimum-energy path for insertion and subsequent protonolysis. In general, the two stereoisomers related to the different diene enantiofaces were found to be close in energy for each of the species. Herein, however, only the favorable one was reported.

[1] a) R. Ahlrichs, M. Bär, M. Häser, H. Horn, C. Kölmel, C. *Chem. Phys. Lett.* **1989**, *162*, 165; b) O. Treutler, R. Ahlrichs, *J. Chem. Phys.* **1995**, *102*, 346; c) K. Eichkorn, O. Treutler, H. Öhm, M. Häser, R. Ahlrichs, *Chem. Phys. Lett.* **1995**, *242*, 652.

[2] a) P. A. M. Dirac, *Proc. Cambridge Philos. Soc.* **1930**, *26*, 376; b) J. C. Slater, *Phys. Rev.* **1951**, *81*, 385; c) S. H. Vosko, L. Wilk, M. Nussiar, *Can. J. Phys.* **1980**, *58*, 1200; d) A. D. Becke, *Phys. Rev.* **1988**, *A38*, 3098; e) J. P. Perdew, *Phys. Rev.* **1986**, *B33*, 8822; *Phys. Rev. B* **1986**, *34*, 7406.

[3] see, for instance: a) S. Tobisch, Th. Nowak, H. Boegel, *J. Organomet. Chem.* **2001**, *619*, 24; b) H. Heiber, O. Gropen, J. K. Laerdahl, O. Swang, U. Wahlgreen, *Theor. Chem. Acc.* **2003**, *110*, 118.

[4] see, for instance: a) S. Tobisch, *Chem. Eur. J.* **2005**, *11*, 3113; b) S. Tobisch, *J. Am. Chem. Soc.* **2005**, *127*, submitted.

[5] M. Dolg, H. Stoll, A. Savin, H. Preuß, *Theor. Chim. Acta* **1989**, *75*, 173.

[6] a) A. Schäfer, C. Huber, R. Ahlrichs, *J. Chem. Phys.* **1992**, *97*, 2571; b) A. Schäfer, C. Huber, R. Ahlrichs, *J. Chem. Phys.* **1994**, *100*, 5829.

[7] W. Koch, M. C. Holthausen, *A Chemist's Guide to Density Functional Theory*, 2nd ed., Wiley-VCH, Weinheim, **2001**.

[8] For further details, see: *www.struked.de*.

[9] D. A. McQuarrie, *Statistical Thermodynamics*, Harper & Row, New York, **1973**.

[10] a) Y. Li, T. J. Marks, *Organometallics* **1996**, *15*, 3770; b) J.-S. Ryu, G. Y. Li, T. J. Marks, *J. Am. Chem. Soc.* **2003**, *125*, 12584; c) typical reaction conditions for the regioselective organolanthanide-mediated intermolecular hydroamination of 1,3-dienes with primary amines are: 49-fold and 29-fold molar excess of 1,3-butadiene and *n*-propylamine **1** reactants, respectively, together with the precatalyst (for example, $Me_2SiCp'_2NdCH(TMS)_2$ **2**) at 60 °C in benzene.

[11] a) J. Tomasi, M. Persico, *Chem. Rev.* **1994**, *94*, 2027; b) C. J. Cramer, D. G. Truhlar, *Chem. Rev.* **1999**, *99*, 2161; c) C. J. Cramer, *Essentials of Computational Chemistry: Theories and Models*; John Wiley & Sons: Chichester, U. K., **2002**, pp 347-383.

[12] *CRC Handbook of Chemistry and Physics*, 3rd electronic ed. (Ed.: D. R. Lide), **2000**; http://www.knovel.com/.

[13] A. Klamt, G. J. Schüürmann, *Chem. Soc., Perkin Trans. 2* **1993**, 799; b) A. Klamt, In *Encyclopedia of Computational Chemistry*, *Vol. 1*, (Ed.: P. von R. Schleyer), Wiley, Chichester, **1998**, pp 604-615.

[14] A. Schäfer, A. Klamt, D. Sattel, J. C. W. Lohrenz, F. Eckert, F. *Phys. Chem. Chem. Phys.* **2000**, *2*, 2187.

[15] A. Klamt, V. Jonas, Th. Bürger, J. C. W. Lohrenz, *J. Phys. Chem. A* **1998**, *102*, 5074.

[16] E. Wilhelm, R. Battino, *Chem. Rev.* **1973**, *73*, 1.

[17] J. Cooper, T. Ziegler, *Inorg. Chem.* **2002**, *41*, 6614.

[18] K. R. Hanson, *J. Am. Chem. Soc.* **1966**, *88*, 2731.

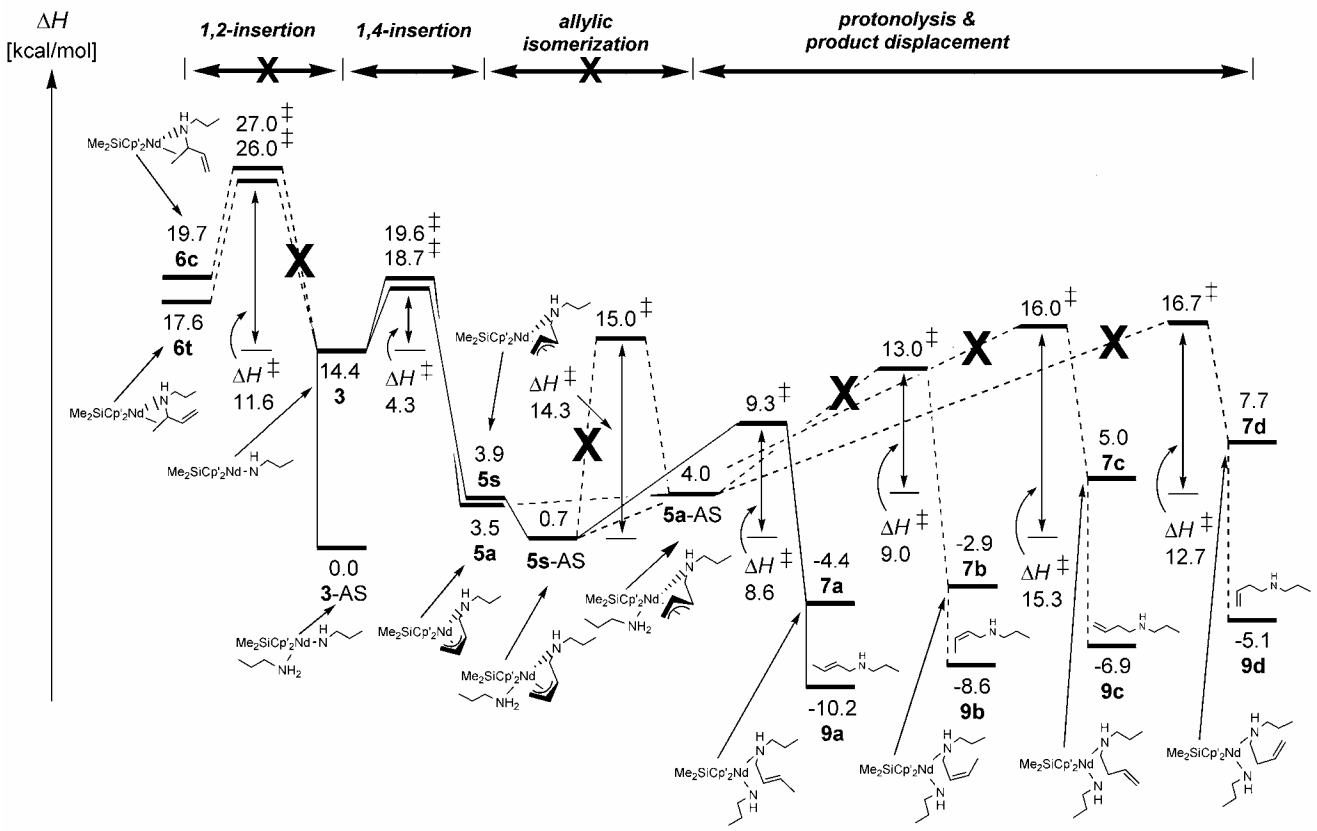

Scheme S1. Condensed enthalpy profile [kcal mol^{-1}] of the intermolecular hydroamination of 1,3-butadiene and *n*-propylamine **1** mediated by $Me_2SiCp'_2NdCH(TMS)_2$ precatalyst **2**. The most feasible pathways for individual steps are drawn by solid lines, while alternative, but unfavorable pathways are represented by dashed lines. Activation enthalpies ($\Delta H^{‡}$) for individual steps are given in kilocalories per mole relative to the respective precursor. Aminoalkene displacement through **7a**/**7b**/**7c**/**7d** + **1** → **3**-AS + **9a**/**9b**/**9c**/**9d** is included.

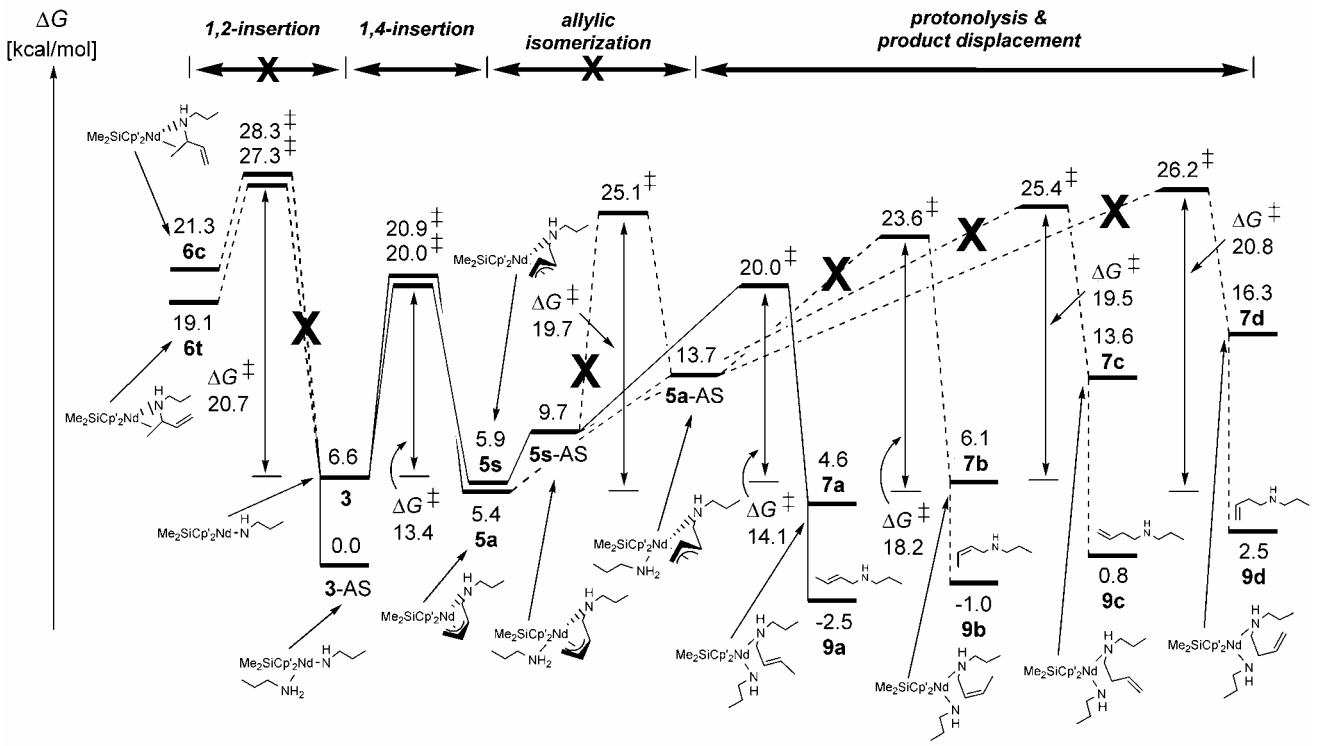

Scheme S2. Condensed Gibbs free-energy profile [kcal mol^{-1}] of the intermolecular hydroamination of 1,3-butadiene and *n*-propylamine **1** mediated by $Me_2SiCp'_2NdCH(TMS)_2$ precatalyst **2**. The most feasible pathways for individual steps are drawn by solid lines, while alternative, but unfavorable pathways are represented by dashed lines. Activation enthalpies ($\Delta G^{‡}$) for individual steps are given in kilocalories per mole relative to the respective precursor. Aminoalkene displacement through **7a**/7**b**/**7c**/**7d** + **1** → **3**-AS + **9a**/**9b**/**9c**/**9d** is included.

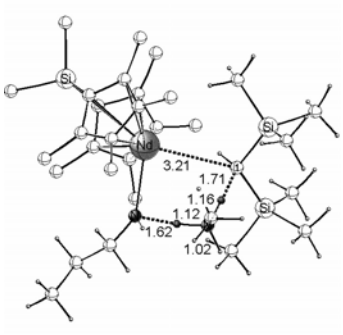

TS[**2**+**1**-$MeNH_2$–**3**+$CH_2(TMS)_2$]

Figure S1. Selected geometric parameters [Å] of the optimized transition-state structure for **1** + **2** → **3** + $CH_2(TMS)_2$ activation of precatalyst **2** through protonolysis by amine **1** that is assisted by methylamine model substrate acting as a 'proton shuttle'. The cutoff for drawing Nd–C bonds was arbitrarily set to 3.1 Å. The hydrogen atoms on the methyl groups of the catalyst backbone are omitted for the sake of clarity.

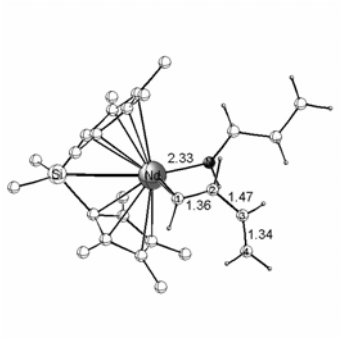

4-1,2c

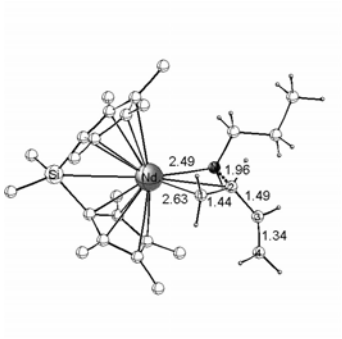

TS[**4**-1,2c–**6c**]

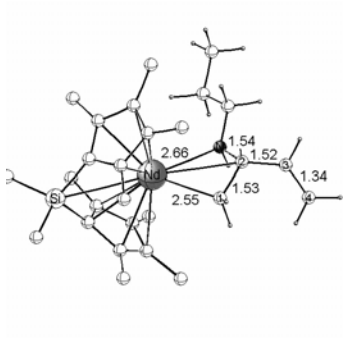

6c

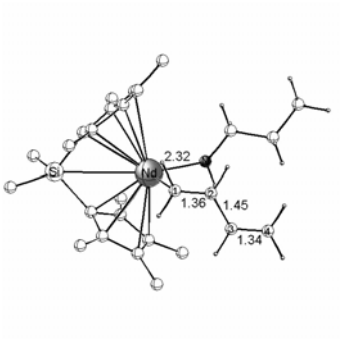

4-1,2t

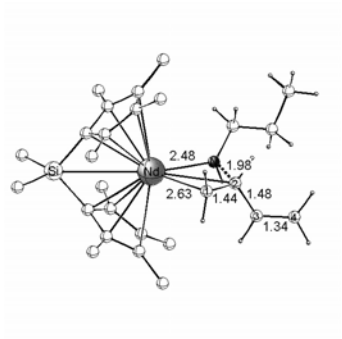

TS[**4**-1,2t–**6t**]

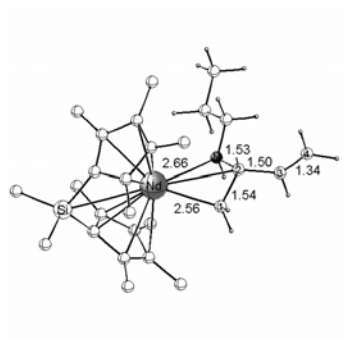

6t

Figure S2. Selected geometric parameters [Å] of the optimized structures of key species for the stereoisomeric *cis*-1,2- (top) and *trans*-1,2-insertion (bottom) pathways. The cutoff for drawing Nd–C bonds was arbitrarily set to 3.1 Å. The hydrogen atoms on the methyl groups of the catalyst backbone are omitted for the sake of clarity.

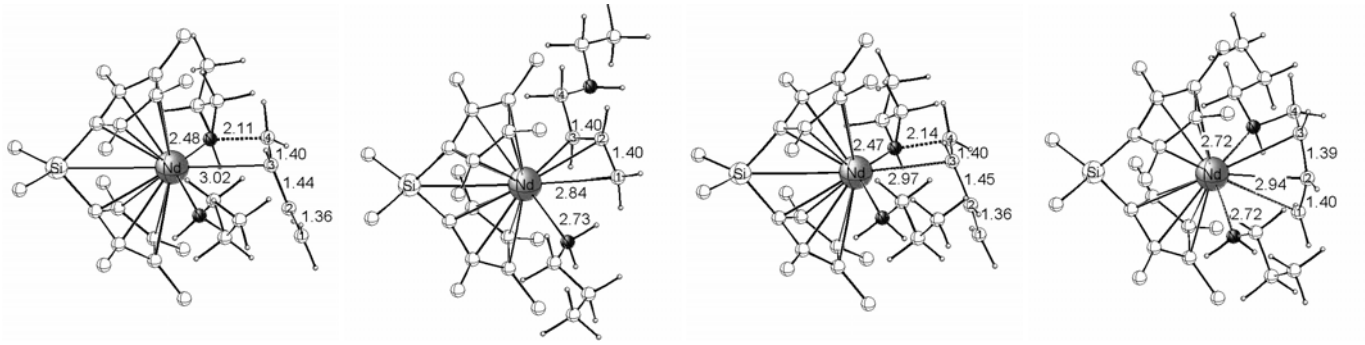

TS[**4**-1,4t–**5s**]-AS **5s**-AS TS[**4**-1,4c–**5a**]-AS **5a**-AS

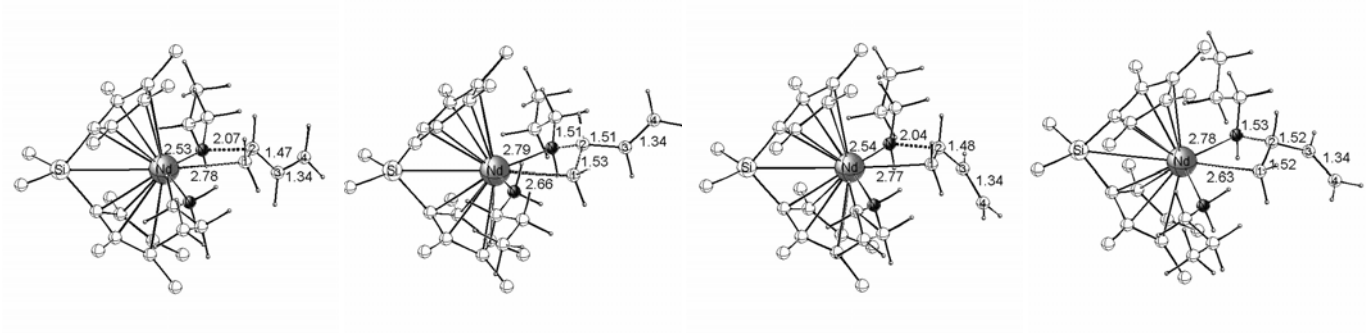

TS[**4**-1,2t–**6t**]-AS **6t**-AS TS[**4**-1,2c–**6c**]-AS **6c**-AS

Figure S3. Selected geometric parameters [Å] of the optimized structures of key species for the regioisomeric 1,4- (top) and 1,2-insertion (bottom) paths to be assisted by amine substrate **1** (AS). The cutoff for drawing Nd–C bonds was arbitrarily set to 3.1 Å. The hydrogen atoms on the methyl groups of the catalyst backbone are omitted for the sake of clarity.

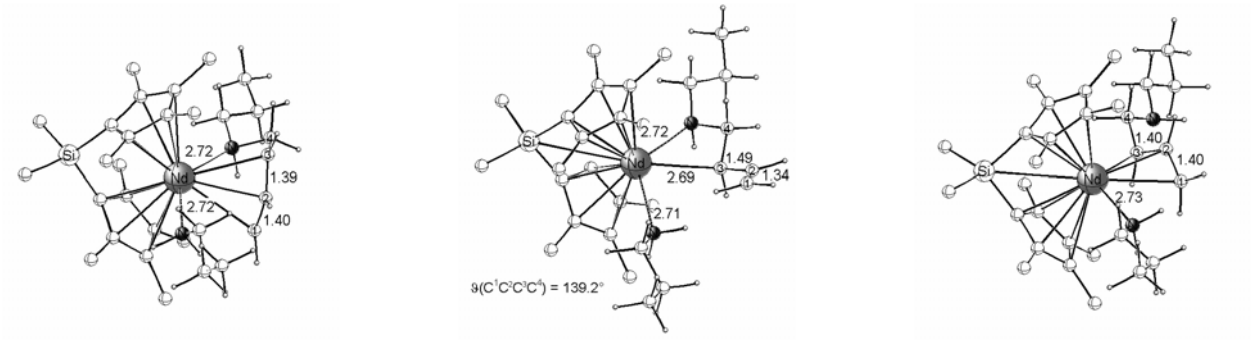

5a-AS TS_{ISO}[**5**]-AS **5s**-AS

Figure S4. Selected geometric parameters [Å, °] of the optimized structures of key species for allylic **5s** ⇄ **5a** isomerization to be assisted by amine substrate **1** (AS). The cutoff for drawing Nd–C bonds was arbitrarily set to 3.1 Å. The hydrogen atoms on the methyl groups of the catalyst backbone are omitted for the sake of clarity.

generation of **7a** *via protonolysis of butenyl-*C^1 *in* **5s**

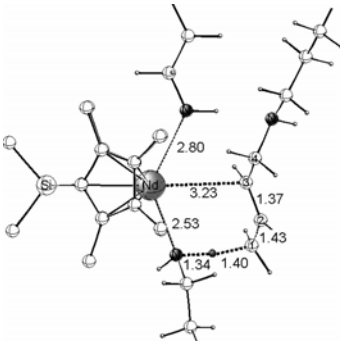

generation of **7c** *via protonolysis of butenyl-*C^3 *in* **5s**

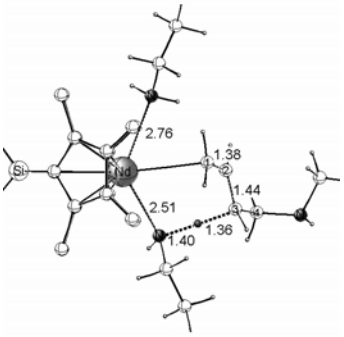

generation of **7b** *via protonolysis of butenyl-*C^1 *in* **5a**

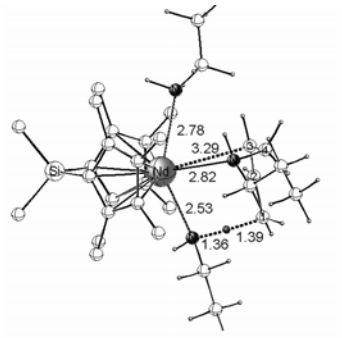

TS[**5**-AS–**7**]-AS

generation of **7d** *via protonolysis of butenyl-*C^3 *in* **5a**

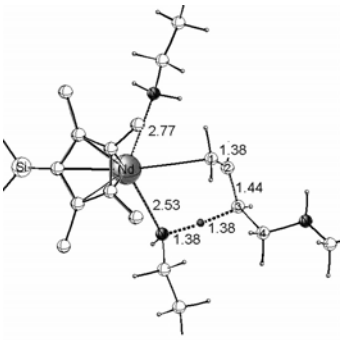

TS[**5**-AS–**7**]-AS

Figure S5. Selected geometric parameters [Å] of the optimized structures of key species for protonolysis of the η^3-butenyl–Nd complex **5** by amine substrate **1** (AS) affording aminoalkene-amido–Nd compounds **7a-7d** along alternative pathways. The cutoff for drawing Nd–C bonds was arbitrarily set to 3.1 Å. The hydrogen atoms on the methyl groups of the catalyst backbone are omitted for the sake of clarity. Please note that several of the species are displayed in a truncated fashion.